14.2 PRECIPITATION, THE REAR FLANK DOWNDRAFT, AND TORNADOES

Mark Askelson*
University of North Dakota, Grand Forks, North Dakota

Jerry Straka
University of Oklahoma, Norman, Oklahoma

Erik Rasmussen
Cooperative Institute for Mesoscale Meteorological Studies, Norman, Oklahoma

1. INTRODUCTION

Given their infrequent occurrence, supercells produce an inordinate amount of death and damage (Moller et al. 1994). Because of this, supercells have been studied intensely for the past forty years.

One of the most damaging aspects of supercells is their proclivity to produce tornadoes. Consequently, the development of tornadoes, or tornadogenesis, is an active research topic. In the past twenty years or so, the rear flank downdraft (RFD; Lemon and Doswell 1979) has received significant attention for its potential role in tornadogenesis (Davies-Jones 1982; Davies-Jones and Brooks 1993; Walko 1993; Davies-Jones 2000; Markowski 2002; Markowski et al. 2002). This has been motivated by numerous studies, including those of Rotunno and Klemp and (1985) and Davies-Jones and Brooks (1993), in which significant low-level rotation does not develop in numerical simulations when hydrometeor production is turned off.

As summarized by Davies-Jones et al. (2001), the development of low-level rotation in association with an RFD can occur through either baroclinic or barotropic processes. In the baroclinic mechanism, the RFD produces horizontal buoyancy gradients that generate horizontal vorticity that is subsequently tilted into the vertical. In the barotropic mechanism, a leading theory is that the RFD generates vertical vorticity by tilting pre-existing horizontal vorticity. Thus, both the dynamic and thermodynamic properties of the RFD appear to be potentially important to tornadogenesis.

With regards to the proposed baroclinic and barotropic tornadogenesis mechanisms, the findings of Markowski et al. (2002) are intriguing. They found that surface RFD air associated with strong supercellular tornadoes (≥F2 intensity and lasting >5 minutes) is relatively buoyant (θ_v and θ_e deficits relative to the environment typically <2 K and <4 K, respectively) while surface RFD air associated with non-tornadic supercells tends to have little buoyancy (θ_v and θ_e deficits relative to the environment typically >5 K and >10 K, respectively). Thus, these findings underscore the importance of RFD thermodynamic properties and support a barotropic tornadogenesis mechanism.

* *Corresponding author address*: Mark A. Askelson, University of North Dakota, Dept. of Atmospheric Sciences, P.O. Box 9006, Grand Forks, ND 58202-9006; e-mail: askelson@aero.und.edu.

Because of the apparent importance of dynamic and thermodynamic properties of RFDs to tornadogenesis, these are studied for a variety of prescribed environments using a 1.5-dimension downdraft model. The spatial dimensionality of this model is purposely less than three so as to simplify analyses and to focus on vertical processes, which are thought to be of primary importance. Moreover, prescribed environments are used so as to span a wide range of conditions that both incorporate the range of perceived possible RFD environments and to illustrate different modes of modeled RFD behavior. A description of the model is provided next, followed by a description of prescribed environments, results, discussion, and conclusions.

2. 1.5 DIMENSION DOWNDRAFT MODEL

In the following sections, information regarding the downdraft model used herein is provided. For more detailed information, see Askelson (2002).

2.1 *Dynamics*

The dynamic framework follows that of Asai and Kasahara (1967), Ogura and Takahashi (1971), and Ogura and Takahashi (1973). The downdraft is assumed to be circular and to have a time- and height-independent radius a. By using cylindrical coordinates, the anelastic continuity equation to express equations in flux form, averaging across the area of the downdraft, and parameterizing lateral mixing as continuous and homogeneous, equations take on forms similar to the following for vertical velocity *w*

$$\frac{\partial \overline{w}}{\partial t} = -\overline{w}\frac{\partial \overline{w}}{\partial z} - \frac{2\alpha^2}{a}|\overline{w}|\overline{w} + \frac{2}{a}\widetilde{u}_a(\overline{w} - \widetilde{w}_a) + B\,, \qquad (1)$$

where the overbar indicates the areal average across the downdraft, α^2 is the lateral mixing coefficient, tildes with a subscript a represent the average value along the boundary of the downdraft at an altitude *z*, *B* is buoyancy (a source term), and $w = 0$ is assumed in the model environment. The first term on the rhs of (1) is advection, the second mixing owing to lateral eddy exchange, and the third is dynamic entrainment associated with mass continuity. Inflow/outflow at the downdraft edges $\widetilde{u}_a$, which accounts for the ".5" in "1.5

dimensional model", is diagnosed from the continuity equation

$$\tilde{u}_a = -\frac{a}{2}\left(\frac{\overline{w}}{\rho_0}\frac{\partial \rho_0}{\partial z} + \frac{\partial \overline{w}}{\partial z}\right), \quad (2)$$

where ρ is density and subscript zeros indicate environmental values. The corresponding equation for temperature T is

$$\frac{\partial \overline{T}}{\partial t} = -\overline{w}\left(\frac{\partial \overline{T}}{\partial z} + \Gamma_d\right) - \frac{2\alpha^2}{a}|\overline{w}|(\overline{T} - T_0) + \frac{2}{a}\tilde{u}_a(\overline{T} - \tilde{T}_a) + \frac{q}{c_p}, \quad (3)$$

where Γ_d is the dry adiabatic lapse rate, q is the specific heating rate, and c_p is the specific heat capacity of dry air at constant pressure.

The conservation equations for water vapor mixing ratio r_v and cloud water mixing ratio r_c are

$$\frac{\partial \overline{r}_v}{\partial t} = -\overline{w}\frac{\partial \overline{r}_v}{\partial z} - \frac{2\alpha^2}{a}|\overline{w}|(\overline{r}_v - r_{v0}) + \frac{2}{a}\tilde{u}_a(\overline{r}_v - \tilde{r}_{va}) + S_{rv\_\mathrm{cond}} \quad (4)$$

and

$$\frac{\partial \overline{r}_c}{\partial t} = -\overline{w}\frac{\partial \overline{r}_c}{\partial z} - \frac{2\alpha^2}{a}|\overline{w}|\overline{r}_c + \frac{2}{a}\tilde{u}_a(\overline{r}_c - \tilde{r}_{ca}) + S_{rc\_\mathrm{cond}}, \quad (5)$$

where S_{rv_cond} and S_{rc_cond} are sources/sinks for r_v and r_c owing to condensation/evaporation. In (5), the fall speeds of cloud droplets are ignored and the environment is assumed to be non-cloudy.

Because details of rain and graupel/hail size distributions can be important to downdraft properties (Srivastava 1985, 1987), the prognostic variables for rain and graupel/hail are number concentration densities—the number of hydrometeors of a certain size per unit volume per unit size interval. The prognostic equations are

$$\begin{aligned}\frac{\partial \overline{N}(D_r)}{\partial t} = &-(\overline{w} - v_{tr})\frac{\partial \overline{N}(D_r)}{\partial z} + \overline{N}(D_r)\frac{\overline{w}}{\rho_0}\frac{\partial \rho_0}{\partial z} - \frac{2\alpha^2}{a}|\overline{w}|\overline{N}(D_r) \\ &+ \frac{2}{a}\tilde{u}_a\left[\overline{N}(D_r) - \tilde{N}_a(D_r)\right] + \overline{N}(D_r)\frac{\partial v_{tr}}{\partial z} \\ &+ S_{\overline{N}(D_r)\_\mathrm{evap}} + S_{\overline{N}(D_r)\_\mathrm{melt}}\end{aligned} \quad (6)$$

and

$$\begin{aligned}\frac{\partial \overline{N}(D_{gh})}{\partial t} = &-(\overline{w} - v_{tgh})\frac{\partial \overline{N}(D_{gh})}{\partial z} + \overline{N}(D_{gh})\frac{\overline{w}}{\rho_0}\frac{\partial \rho_0}{\partial z} - \frac{2\alpha^2}{a}|\overline{w}|\overline{N}(D_{gh}) \\ &+ \frac{2}{a}\tilde{u}_a\left[\overline{N}(D_{gh}) - \tilde{N}_a(D_{gh})\right] + \overline{N}(D_{gh})\frac{\partial v_{tgh}}{\partial z} \\ &+ S_{\overline{N}(D_{gh})\_\mathrm{cond}} + S_{\overline{N}(D_{gh})\_\mathrm{melt}}\end{aligned}, \quad (7)$$

where $N(D_r)$ is the number of drops of diameter D_r per unit volume per unit size interval, v_{tr} is the terminal velocity of a raindrop of diameter D_r, $S_{\overline{N}(D_r)\_\mathrm{evap}}$ is the source/sink of $\overline{N}(D_r)$ owing to evaporation, $S_{\overline{N}(D_r)\_\mathrm{melt}}$ is the source/sink of $\overline{N}(D_r)$ owing to the complete melting of ice hydrometeors, $N(D_{gh})$ is the number of graupel/hail of diameter D_{gh} per unit volume per unit size interval, v_{tgh} is the terminal velocity of a graupel/hailstone of diameter D_{gh}, $S_{\overline{N}(D_{gh})\_\mathrm{cond}}$ is the source/sink of $\overline{N}(D_{gh})$ owing to condensation/evaporation, and $S_{\overline{N}(D_{gh})\_\mathrm{melt}}$ is the source/sink of $\overline{N}(D_{gh})$ owing to melting. As with cloud water, the environment is assumed to contain neither rain nor graupel/hail.

In formulating the model equations, exchanges owing to vertical eddy fluxes are disregarded. In addition, *since there is no mechanism for the computation of perturbation pressures in this model (Ogura and Takahashi 1971), they have been disregarded*. Buoyancy is thus given by

$$B = g\left(\frac{T_v'}{T_{v0}} - r_H\right), \quad (8)$$

where g is the acceleration due to gravity, T_v is virtual temperature, and r_H is the total hydrometeor mixing ratio. Since perturbation pressures are disregarded, *downdrafts are generated only as a result of hydrometeor forcing*.

2.2 *Microphysics*

In (6) and (7), the terminal velocities of raindrops and graupel/hail are needed. A discussion of this remarkably challenging problem is provided in Askelson (2002). As a compromise between more exact, complex formulations and less exact, simple formulations, an adjustment-factor approach is used herein. Thus, the terminal velocities of raindrops are given by

$$v_{tr}(D_r, \rho) = v_{tr0}(D_r)(\rho_0/\rho)^{0.45} \quad (9)$$

where v_{tr0} is the terminal velocity at a reference density ρ_0.* The terminal velocities of graupel/hail are given by

$$v_{tgh}(D_{gh}, \rho) = v_{tgh0}(D_{gh})(\rho_0/\rho)^{0.42}, \quad (10)$$

where v_{tgh0} is the terminal velocity of a graupel or hailstone at the reference density ρ_0. The v_{tr0} relation is from Atlas et al. (1973) and is given by

$$v_{tr0}(D_r) = [9.65 - 10.3\exp(-0.6D_r)], \quad (11)$$

where D_r is in mm, v_{tr0} is in m s^{-1}, and for which ρ_0 = 1.2 kg m^{-3}. Following Askelson (2002), v_{tgh0} is given by

* Note that for the terminal velocity equations discussed in this section, a subscript zero indicates a reference value as opposed to an environmental value.

$$v_{tgh0}(D_{gh}) = 11.6 D_{gh}^{0.71}, \quad (12)$$

where v_{tgh0} is in m s^{-1}, D_{gh} is in cm, and ρ_0 = 0.993 kg m^{-3}.

The source/sink term S_{rc_cond}, the source/sink of r_c owing to condensation/evaporation, is handled using the Soong and Ogura (1973) saturation adjustment scheme. Other important microphysical processes include the evaporation of raindrops, condensation/evaporation at the surfaces of melting graupel/hailstones, graupel/hailstone melting, and shedding of melting graupel/hailstones. Evaporation of rain is computed using equations that are commonly applied to this process (e.g., Rogers and Yau 1989, chapter 7). The formulations of graupel/hail evaporation/condensation, melting, and shedding follow those of Rasmussen and Heymsfield (1987). Rates of change owing to these processes are used to compute S_{rv_cond}, $S_{\overline{N}(D_r)\_evap}$, $S_{\overline{N}(D_r)\_melt}$, $S_{\overline{N}(D_{gh})\_cond}$, and $S_{\overline{N}(D_{gh})\_melt}$. The details, which are omitted here for brevity, are provided in Askelson (2002).

It is noted that hydrometeor collision, collection, and breakup processes are not included in this model since they are not expected to change the fundamental behavior of modeled downdrafts. Moreover, this model is designed for relatively low-level downdrafts in which graupel and hailstones are melting and thus have ice cores surrounded by liquid water shells (Rasmussen et al. 1984).

2.3 *Initialization*

The environment of the model is initialized assuming hydrostatic conditions, which is needed to determine p at each model level, with no cloud droplets, raindrops, or graupel/hail. As discussed in section 3, three different types of soundings, Srivastava, pseudoadiabatic, and cap, are considered herein. For Srivastava soundings, the critical assumption is that T_v varies linearly with ln$p$, which is a commonly applied assumption when heights are computed from sounding data (Richner and Viatte 1995) and results in a hypsometric equation that is implicit in p and must be solved numerically. For pseudoadiabatic soundings, p at each model level is determined by numerically integrating the hydrostatic equation. For cap soundings, T and r_v are assumed to vary linearly with height. With the use of $T_v \approx T(1 + .608 r_v)$, the hydrostatic equation can then be integrated to produce explicit equations for p. Note that in pseudoadiabatic soundings, environmental conditions below the convective condensation level (CCL) are computed using the same methods applied to cap soundings.

At their level of insertion, raindrops are assumed to conform to an exponential distribution while graupel/hail are assumed to conform to a Cheng-English exponential distribution (Cheng and English 1983; Cheng et al. 1985). Unless otherwise noted, the input rain and graupel/hail fields contribute nearly equally to a combined reflectivity at horizontal polarization of Z_h = 50 dBZ, with the intercept and slope parameters of the input rain field being N_{0r} = 1171.1 m^{-3} mm^{-1} and Λ_r = 1.59 mm^{-1}, respectively, and the slope parameter of the input graupel/hail field being Λ_{gh} = 1.019 mm^{-1}. A separate intercept parameter does not need to be specified for graupel/hail since in the Cheng-English exponential distribution, the intercept and slope parameters are related. The maximum hail diameter is 2 cm.

2.4 *Boundary Conditions, Initial Conditions, Solution Methods, and Parameters*

At the upper and lower boundaries, all model variables, excluding $\overline{w}$, are allowed to evolve through the various processes outlined above. For $\overline{w}$, rigid boundary conditions are applied, with $\overline{w} = 0$ at the upper and lower boundaries. Since updrafts do not impact the upper boundary in these simulations, the rigid upper boundary condition for $\overline{w}$ has little impact. The $\overline{w} = 0$ condition at the surface, however, enforces the dynamic boundary condition there.

At time zero, all model fields, except for rain and graupel/hail at one altitude, are equal to environmental values. Rain and graupel/hail fields are inserted at one altitude at each time step, including time step zero. This is consistent with steady hydrometeor production in storms. Situations in which hydrometeor fields that drive RFDs evolve are not considered.

Unless otherwise noted, hydrometeor fields are inserted into the model at an altitude of 2.1 km agl. This level is low enough to ensure that graupel/hail are melting and high enough so that relations between downdraft properties and low-level sounding features can be illustrated.

Finite differences are used. They are forward in time, upstream for advection terms, and centered in space for non-advection terms. The grid spacing is 0.1 km and the time step is 0.5 s. The finite differences, grid spacing, and time step are all similar to those used by Srivastava (1985, 1987). Tests were performed to ensure numerical convergence.

Fifty rain and graupel/hail size bins are used. Following Ogura and Takahashi (1971), $\alpha^2 = 0.1$, which is an appropriate value for jets and starting plumes (Houze 1993, §7.3.2). The radius of the downdrafts a is set at 3 km. This is approximately in the middle of the size range given by Knupp and Cotton (1985) for precipitation-driven downdrafts.

3. PRESCRIBED ENVIRONMENTS

Prescribed environments are used so as to span a range of perceived possible RFD environments and to illustrate different modes of modeled RFD behavior. The first type of prescribed environment is the Srivastava environment, so named because it was used in tests performed by Srivastava (1985, 1987). In this environment, surface temperature, surface pressure, a

temperature lapse rate that is constant throughout the atmosphere, and a relative humidity that is constant throughout the atmosphere, are prescribed. This type of environment is used to underscore simple characteristics of precipitation-driven downdrafts.

The second type of environment that is used is pseudoadiabatic. In this environment, conditions are pseudoadiabatic at and above the CCL of surface air parcels. Below the CCL, the temperature lapse rate is dry adiabatic so as to avoid unstable dry motions within a model layer below the CCL, which would occur if the temperature lapse rate were less than dry adiabatic below the CCL, and unstable dry motions throughout the layers below the CCL, which would occur if the temperature lapse rate were greater than dry adiabatic below the CCL. Below the CCL, r_v varies linearly with height, with the constraint that $dr_v/dz < 0$ so that saturated conditions are not reached below the (prescribed) CCL. This type of environment is used because it can be argued that conditions within the updraft may typify the environment of the downdraft.

The third type of environment used is the cap environment. This environment is used because environmental supercell soundings oftentimes have a layer characterized by a low temperature lapse rate that resides immediately above an atmospheric boundary layer typified by a temperature lapse rate that is or is nearly dry adiabatic (Askelson 2002). The presence of such a capping layer is what delays convective initiation until a forcing mechanism (e.g., convergence) is able to initiate it. This type of sounding is considered because an appropriate environment for the RFD may be that of the overall storm. In this environment, surface pressure, surface temperature, surface dewpoint temperature, dT/dz below, in, and above the cap, and dr_v/dz below, in, and above the cap, are specified. Values of dr_v/dz are constrained such that saturation is not reached within any of the layers.

4. RESULTS

The first results, which are shown in Fig. 1, are provided simply to underscore the importance of temperature lapse rate to downdraft generation and maintenance. As Figs. 1a,b show, the simulated downdraft is much more vigorous for the dry-adiabatic temperature lapse rate (a) than it is for the lesser temperature lapse rate of 6.5 ˚C km^{-1} (b). Moreover, for the dry-adiabatic environment, the downdraft accelerates throughout its descent whereas in the other case the downdraft reaches a near steady state value of 1 m s^{-1}. These behaviors are well known and owe to the fact that precipitation-driven downdrafts descend with temperature lapse rates that are between dry and moist adiabatic (Das and Subba Rao 1972). Consequently, the closer the environmental temperature lapse rate is to dry adiabatic, the more negatively buoyant a downdraft will be, all else being equal. Previous work has illustrated the strong dependence of downdraft strength upon temperature lapse rate (e.g., Kamburova and Ludlam 1966). While temperature lapse rate is a critical factor that helps govern downdraft strength, it is not the only factor. Downdrafts also exhibit sensitivity to hydrometeor characteristics like size distributions and liquid- and ice-water contents (e.g., Srivastava 1987).

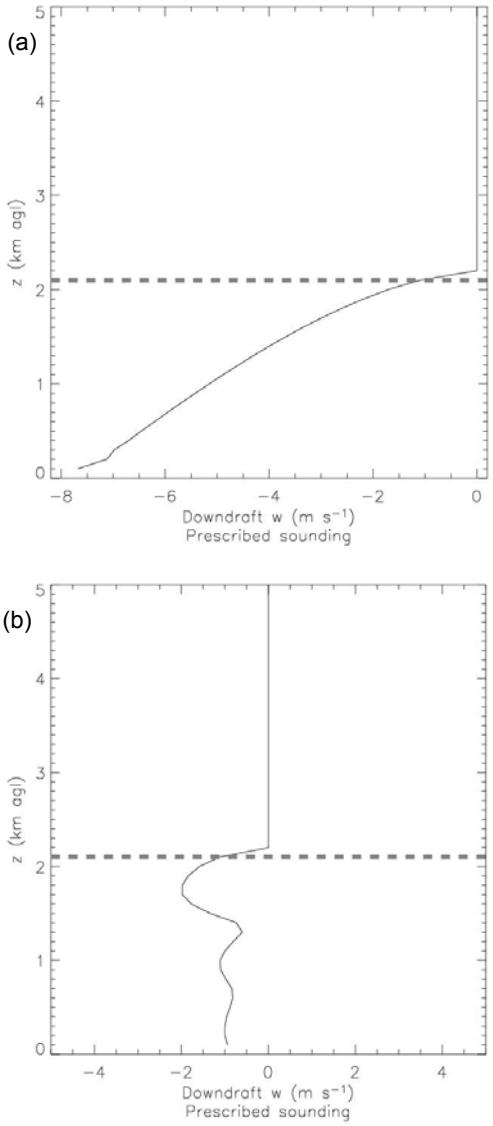

Fig. 1: Downdraft strength as a function of height at t = 30 min for two Srivastava soundings, one having a dry adiabatic temperature lapse rate (a) and the other having a temperature lapse rate of 6.5 ˚C km^{-1} (b). In both simulations, the environmental surface pressure is 1000 mb, the environmental surface temperature is 26.67 ˚C (~80 ˚F), and the environmental relative humidity is 50%. The thick-dashed line indicates the precipitation release altitude. Parameters of input hydrometeor fields are: Z_h = 50 dBZ, N_{0r} = 1171.1 m^{-3} mm^{-1}, Λ_r = 1.59 mm^{-1}, and Λ_{gh} = 1.019 mm^{-1}.

Results for pseudoadiabatic soundings are provided in Figs. 2 and 3. As is apparent in Fig. 2a, the simulated downdraft becomes established only below the CCL. Above the CCL, the environmental temperature lapse rate associated with the θ_{ep} = 340.23

K pseudoequivalent potential temperature (Emanuel 1994, §4.7; Bolton 1980) of this simulation is too small for a significant downdraft to develop. Below the CCL, however, the temperature lapse rate is dry adiabatic and a downdraft develops readily. It is noted that evidence regarding the difficulty in establishing a downdraft above the CCL is provided not only by the strength of the downdraft there but also by its variability. Above the CCL, the downdraft exhibits oscillations and even reverses sign, resulting in areas of weak updraft. These oscillations and weak updrafts result from buoyancy oscillations that arise because downdraft air parcels overshoot their levels of neutral buoyancy.

As indicated earlier, Markowski et al. (2002) found that surface RFD θ_e and θ_v deficits seem to be indicators of tornado potential (their θ_e is equivalent to θ_{ep} used herein). For this study, attention is focused on θ_{ep} deficits, which for the simulation illustrated in Fig. 2 are shown in Fig. 2b. It is important to note that since the temperature lapse rate below the CCL is dry adiabatic and since dr_v/dz = 0.0 g kg^{-1} km^{-1} below the CCL, environmental θ_{ep} does not change with height in this simulation. Thus, one would expect that the downdraft would not be able to produce θ_{ep} deficits near the surface since there are no lower θ_{ep} values to draw upon. This indeed is the case. However, some θ_{ep} deficits do arise in the simulated downdraft. While the exact cause of these is unknown, their correspondence to the levels in which significant melting of graupel/hail occurs (not shown) suggests that they are related to the melting of graupel and hail, processes which are not included in the definition of θ_{ep}. This assertion is further supported by results of a simulation in which all parameters are the same as in Fig. 2 except that all of the precipitation is in the form of rain. In this simulation, downdraft θ_{ep} deficits are minimal (not shown).

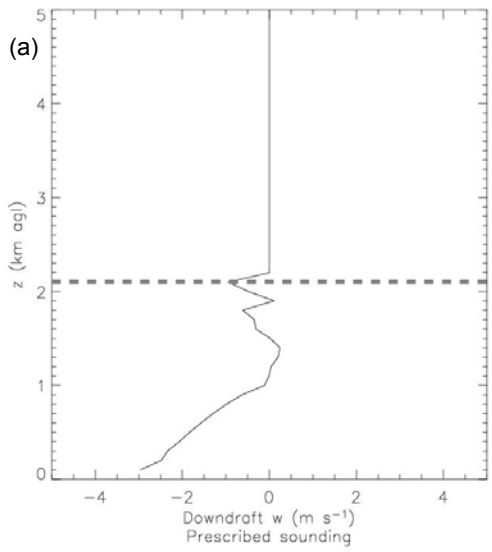

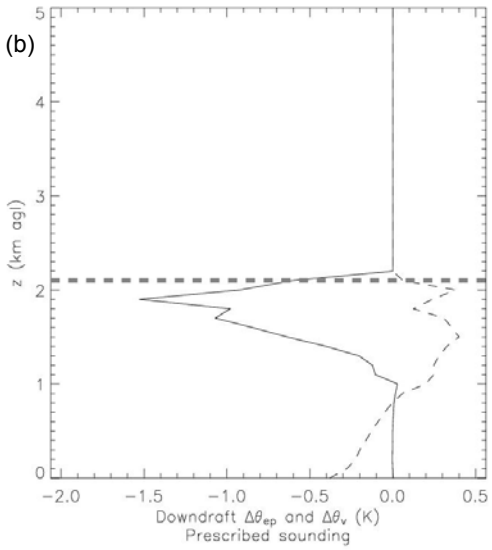

Fig. 2: As in Fig. 1, except for one pseudoadiabatic simulation at t = 30 min for which the CCL is at 1.0 km agl, the temperature lapse rate below the CCL is dry adiabatic, and dr_v/dz = 0.0 g kg^{-1} km^{-1} below the CCL. (a) Downdraft strength versus height. (b) Downdraft θ_{ep} – environmental θ_{ep} (solid line) and downdraft θ_v – environmental θ_v (dashed line) as a function of height. Pseudoequivalent potential temperature θ_{ep} (Emanuel 1994, §4.7) is computed using the formulation of Bolton (1980) and θ_v is computed using $\theta_v = T_v\left(\frac{1000\ \text{mb}}{p}\right)^{R_d/c_p}$.

The parameters for the simulation results shown in Fig. 3 are equivalent to those for the simulation illustrated in Fig. 2 with the exception that below the CCL dr_v/dz = -5.0 g kg^{-1} km^{-1}. Because r_v decreases at a significant rate below the CCL, θ_{ep} decreases significantly in this layer (Fig. 3b). Thus, in contrast to the simulation illustrated in Fig. 2, the downdraft has the ability to draw lowered θ_{ep} values to the surface, which it does (Fig. 3c). Because θ_{ep} decreases significantly in the layer in which the downdraft develops and accelerates and because this layer is adjacent to the surface, lower θ_{ep} values are drawn to the surface and, according to the findings of Markowski et al. (2002), this environment has less potential for tornadic development than does the environment of the simulation illustrated in Fig. 2. It is noted that even though downdraft exists throughout the below-CCL layer in which θ_{ep} decreases by about 16 K, the surface downdraft θ_{ep} deficit is only ~8 K. The reasons the surface downdraft θ_{ep} deficit is smaller than its potential 16 K value are mixing owing to lateral eddy exchange and dynamic entrainment owing to mass continuity. The latter is especially important, since the acceleration of the downdraft below the CCL requires significant intake of environmental air. Finally, it is noted that the downdraft in Fig. 3a is stronger than that in Fig. 2a because r_v is lower below the CCL for the simulation depicted in Fig. 3, which results in stronger downdraft forcing through the evaporation of raindrops.

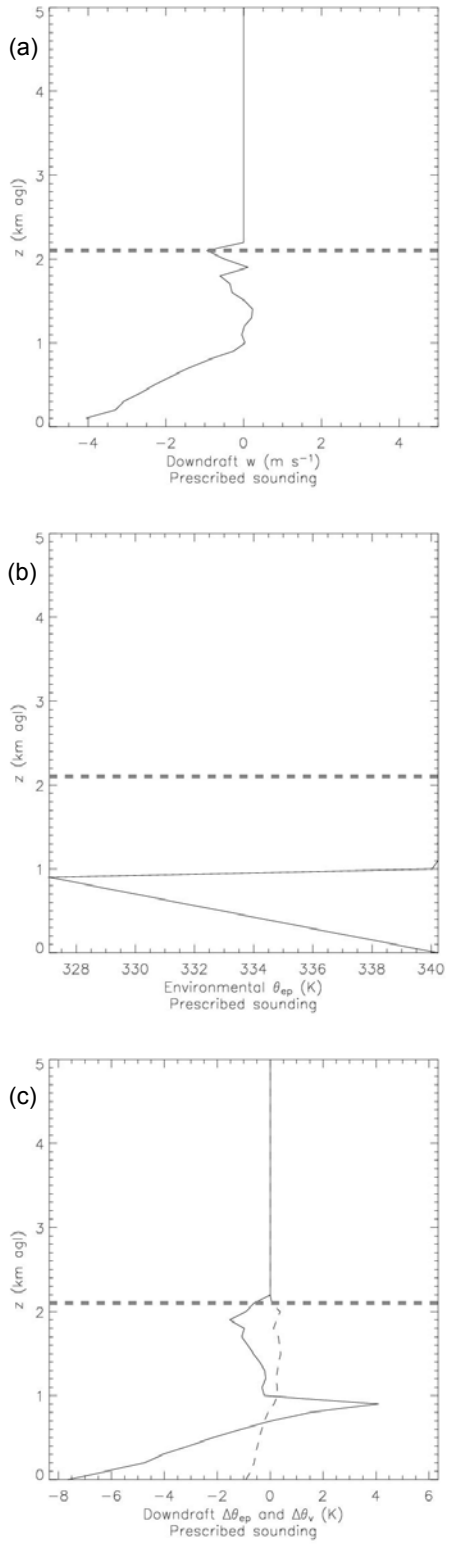

Fig. 3: As in Fig. 2, except (b) illustrates the environmental θ_{ep} profile, (c) provides θ_{ep} and θ_v deficits, and dr_v/dz = -5.0 g kg^{-1} km^{-1} below the CCL.

The results for the first cap sounding simulation are provided in Fig. 4. As illustrated in Fig. 4a, the downdraft is modest above the cap layer (1.0 to 1.1 km agl) where the temperature lapse rate is 7.0 ˚C km^{-1}, is halted in the relatively shallow cap layer where the temperature lapse rate is 0.0 ˚C km^{-1}, and subsequently develops rapidly in the layer below the cap where the temperature lapse rate is dry adiabatic. Because r_v is constant within the layer below the cap, θ_{ep} is constant in this layer (Fig. 4b). Thus, because the cap does not allow the downdraft to draw upon the reservoir of lower θ_{ep} values above it, surface downdraft θ_{ep} deficits are minimal and, according to the findings of Markowski et al. (2002), this sounding should be thermodynamically supportive of tornadogenesis.

Results for a cap-sounding simulation in which θ_{ep} decreases rapidly below and within the cap are provided in Fig. 5. In this simulation, the downdraft structure is similar to that illustrated in Fig. 4a, with a modest downdraft halted by the cap and then developing significantly below the cap. In contrast to the simulation illustrated in Fig. 4, the downdraft is stronger owing to the lower r_v values in this simulation. The biggest differences relative to the simulation illustrated in Fig. 4, however, are the significant low-level θ_{ep} deficits (Fig. 5c). These arise because θ_{ep} decreases considerably in the layer adjacent to the surface and because the downdraft is relatively strong in this layer. Relative to the environment of the Fig. 4 simulation, this environment should be much less likely to support tornadoes.

Figure 6 illustrates what happens when the cap is removed. In this simulation, the temperature lapse rate is dry adiabatic throughout, with r_v constant below the cap, decreasing slightly within the cap, and decreasing rapidly above the cap. These parameters result in θ_{ep} values that are constant below the (functionally non-existent) cap and that decrease in and above the cap (Fig. 6b). With no cap functionally in place, the downdraft extends from the precipitation release altitude to the surface and accelerates throughout this whole layer (Fig. 6a). Moreover, with no cap to halt the downdraft, low θ_{ep} air is drawn from above the cap to the surface (Fig. 6c), despite constant θ_{ep} values below the cap. According to the findings of Markowski et al. (2002), this type of sounding would not be as likely to support tornadogenesis.

Finally, Fig. 7 provides an example of the dependence of downdraft properties on microphysical parameters. All parameters for this simulation are as in Fig. 4 except the microphysical parameters for the input hydrometeor fields correspond to Z_h = 60 dBZ and dr_v/dz = -7.0 g kg^{-1} km^{-1} above the cap. With these parameters, the downdraft is sustained through the cap (Fig. 7a) and significantly lower θ_{ep} values are transported to the surface (Fig. 7c). In a simulation having the same parameters except for microphysical parameters that correspond to Z_h = 50 dBZ, the downdraft is halted in the cap and significantly lower θ_{ep} values are not drawn to the surface (not shown). Interestingly, this sensitivity depends upon the above-cap dr_v/dz value and does not occur when dr_v/dz = -3.1 g kg^{-1} km^{-1} above the cap, which is the value that was used in the simulation illustrated in Fig. 4.

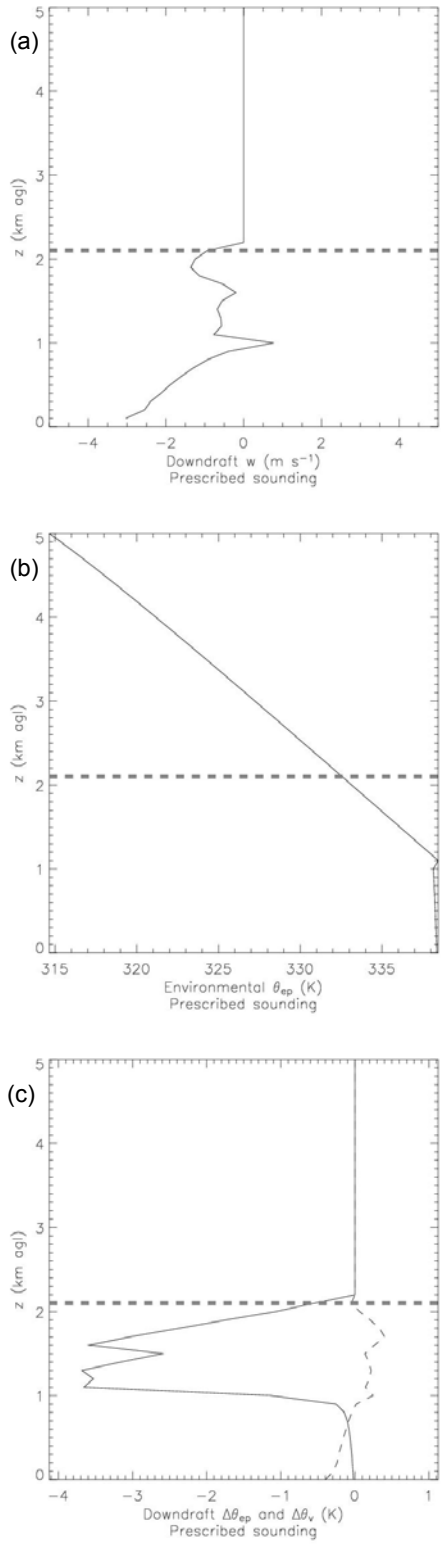

Fig. 4: As in Fig. 3, except for a cap sounding with the following parameters: surface p = 1000 mb, surface T = 26.67 ˚C, surface T_d = 18.0 ˚C, dT/dz below, in, and above cap = -9.767, 0.0, and -7.0 ˚C km^{-1}, respectively, dr_v/dz below, in, and above cap = 0.0, -3.0, and -3.1 g kg^{-1} km^{-1}, respectively, and cap bottom, top altitudes = 1.0 and 1.1 km, respectively.

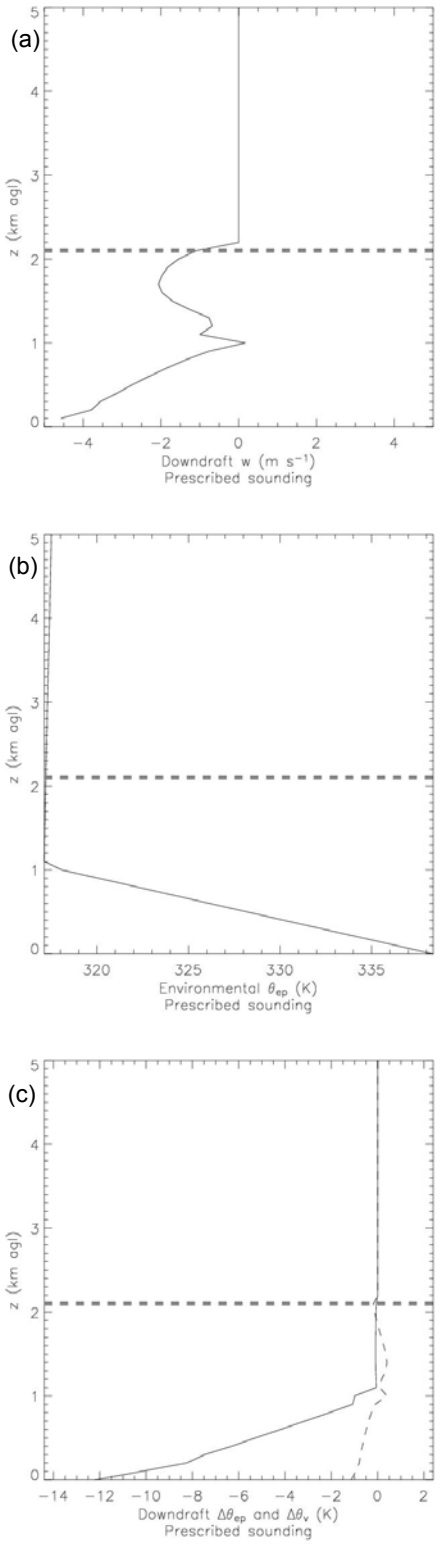

Fig. 5: As in Fig. 4, except dr_v/dz below, in, and above cap = -7.0, -7.0, and -1.0 g kg^{-1} km^{-1}, respectively.

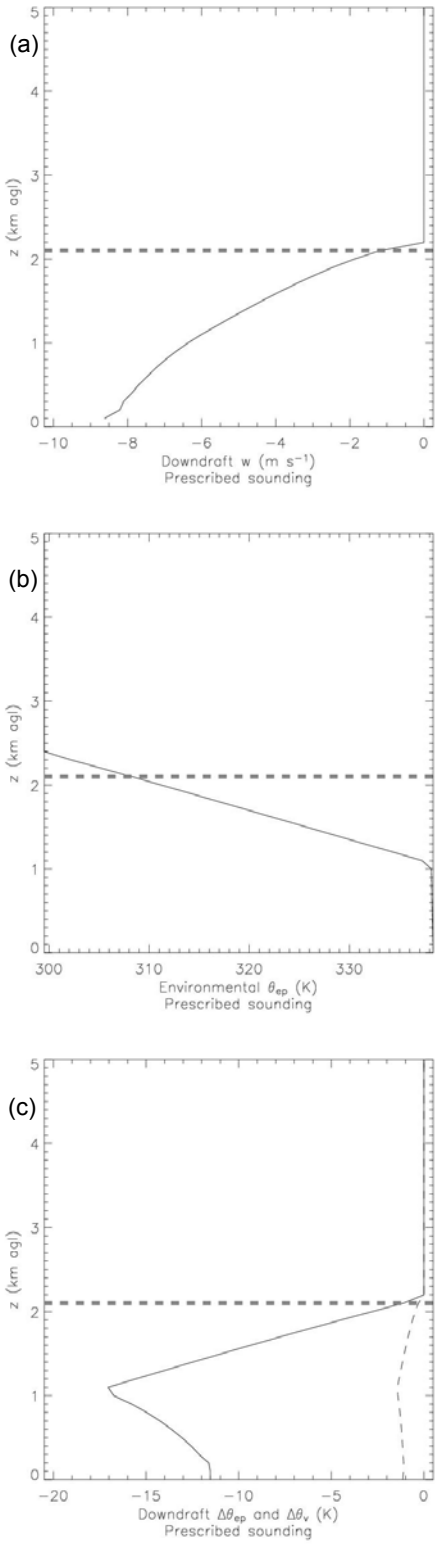

Fig. 6: As in Fig. 4, except dT/dz below, in, and above cap = -9.767 ˚C and dr_v/dz below, in, and above cap = 0.0, -3.0, and -10.0 g kg^{-1} km^{-1}, respectively.

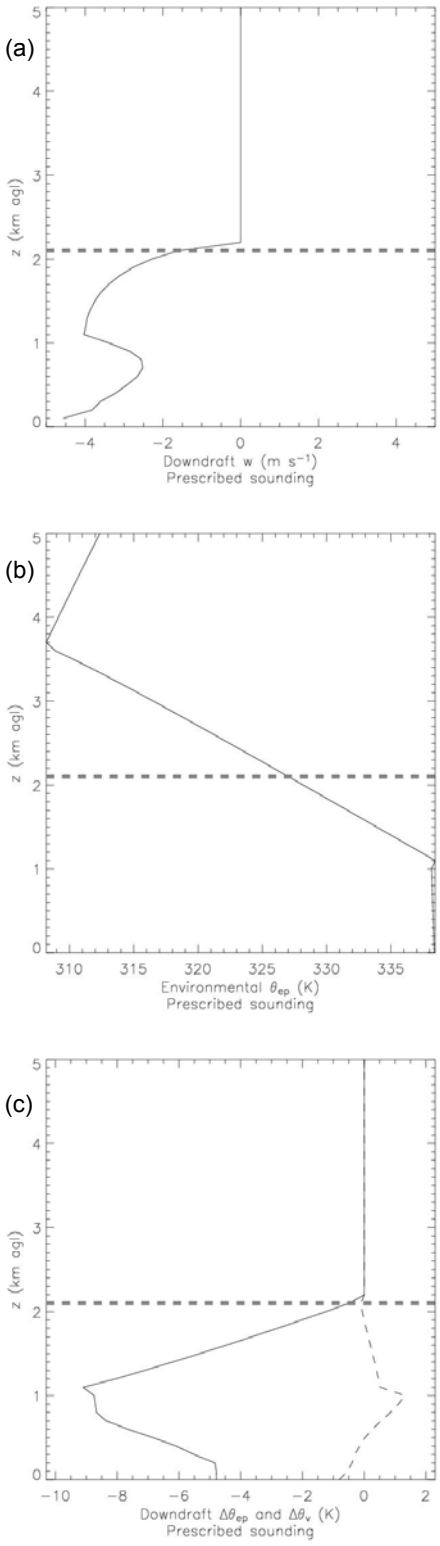

Fig. 7: As in Fig. 4, except dr_v/dz above cap = -5.0 g kg^{-1} km^{-1} and microphysical parameters of input hydrometeor fields are Z_h = 60 dBZ, N_{0r} = 2128.99 m^{-3} mm^{-1}, Λ_r = 1.28 mm^{-1}, and Λ_{gh} = 0.4 mm^{-1}.

DISCUSSION

The soundings that were used in this study were chosen because they are believed to be representative of possible RFD environments. If an RFD environment contains a deep layer of high temperature lapse rate that extends from the surface upward, then that RFD is expected to descend to the surface from relatively high altitudes. This is expected to increase the likelihood that low-θ_{ep} air will descend to the surface and, thus, to decrease the likelihood of tornadogenesis.

RFD environments, however, are not expected to be characterized by a deep layer of high temperature lapse rate that extends from the surface upward. In fact, one may argue that, owing to its proximity to the RFD, updraft conditions are the relevant RFD environmental conditions. Alternatively, the relevant environment may have a layer characterized by a low temperature lapse rate (cap) that resides immediately above an atmospheric boundary layer typified by a temperature lapse rate that is or is nearly dry adiabatic (Askelson 2002). In either case, the dry-adiabatic lapse rates in the boundary layers of these environments result in significant downdrafts in the boundary layer. Moreover, the relatively low temperature lapse rates above the boundary layer in these environments oftentimes prevent air from above the boundary layer from descending to the surface. *Consequently, for many RFDs, boundary layer characteristics may be important to tornado formation*. With regards to θ_{ep} deficits, since temperature lapse rates are dry adiabatic in the boundary layer in these environments, the vertical profile of r_v dictates the vertical profile of θ_{ep} in these boundary layers and, thus, the θ_{ep} deficits that are attainable within an RFD.

Evidence from other studies supports the hypothesis that boundary layer characteristics are important to tornado formation. Markowski et al. (2002) found that surface RFD air oftentimes originated from relatively low altitudes (< 1 km agl), especially in the tornadic cases they studied. This supports the finding herein that RFDs are oftentimes generated and/or enhanced within the boundary layer. Moreover, in studying supercell proximity soundings obtained from the Rapid Update Cycle, Thompson et al. (2003) reinforced findings of earlier studies (e.g., Rasmussen and Blanchard 1998) that low-level moisture parameters such as relative humidity and the Mean Layer Lifted Condensation Level (MLLCL) help to discriminate between significantly tornadic and nontornadic supercells. From the results obtained herein, it seems that the vertical lapse rate of boundary layer r_v, which is related to boundary layer relative humidity and MLLCL, should be studied as a potential tornado discriminator, as should the vertical lapse rate of boundary layer θ_{ep}.

If the barotropic mechanism is important to tornado formation, then because the boundary layer appears to be a very important layer for RFD generation and intensification, shear in this layer could be important to tornado formation. Recent studies (e.g., Rasmussen 2003; Markowski et al. 2003; Thompson et al. 2003) have shown that this, in fact, is the case.

While much of this discussion has focused on the boundary layer, under the right conditions (e.g., weak cap, strong forcing by hydrometeors) relatively high-altitude air having low θ_{ep} values can descend to the surface. This may be an important tornadogenesis failure mechanism. It also complicates the picture somewhat in that determining whether a storm is likely to produce a tornado may depend not only on environmental conditions but also on storm properties such as hook-echo hydrometeor field characteristics.

Finally, it is noted that this study is limited by the fact that a 1.5 dimension model is used. Efforts are currently underway to develop a similar study that uses a three-dimensional, nonhydrostatic model. Such a study would enable the inclusion of effects owing to perturbation pressures and temporally-varying hydrometeor production.

CONCLUSIONS

The following summarize the findings of this work

1) If pseudoadiabatic or cap soundings are representative of RFD environments, it appears as if RFDs are typically either generated or intensified significantly within the boundary layer owing to the dry-adiabatic temperature lapse rate that is usually found there.
2) From 1), if RFDs are typically either generated or intensified significantly within the boundary layer owing to the dry-adiabatic temperature lapse rate that is usually found there, then the boundary layer θ_{ep} profile appears to be very important to surface RFD θ_{ep} deficits and, from the findings of Markowski et al. (2002), to tornadogenesis.
3) From 1) and 2), if the boundary layer θ_{ep} profile is important to tornadogenesis because the temperature lapse rate is typically dry-adiabatic there, then the vertical profile of r_v is important to tornadogenesis since, with a dry-adiabatic temperature lapse rate, it dictates the vertical profile of θ_{ep}.
4) If pseudoadiabatic or cap soundings are representative of RFD environments, then the regions of low temperature lapse rate that reside above the boundary layer in these soundings may be important to tornadogenesis because they oftentimes prevent downdrafts from transporting low-θ_{ep} air from above the boundary layer to the surface. As with updrafts, caps also effectively stifle downdrafts.
5) The ability of a downdraft to penetrate through a cap depends upon both the thermodynamic characteristics of and in the vicinity of the cap and upon the characteristics of the hydrometeor fields that drive the downdraft. Consequently, tornadogenesis may depend upon the characteristics of the hook-echo hydrometeors that help drive the RFD.

6) If RFDs are typically either generated or intensified significantly within the boundary layer owing to the dry-adiabatic temperature lapse rate that is usually found there and a barotropic tornadogenesis mechanism that involves tilting of pre-existing horizontal vorticity is important to tornado formation, then vertical wind shear in the boundary layer should be important to tornadogenesis.

ACKNOWLEDGEMENTS

This work was sponsored by the National Science Foundation under Grant ATM-0003869 and Grant ATM-0340693.

REFERENCES

Asai, T., and A. Kasahara, 1967: A theoretical study of the compensating downward motions associated with cumulus clouds. *J. Atmos. Sci.*, **24**, 487-496.

Askelson, M. A., 2002: Kinematic, dynamic, and thermodynamic impacts of hook-echo hydrometeors, including explorations into the utilization of polarimetric radar data. Ph.D. dissertation, University of Oklahoma, 245 pp.

Atlas, D., R. C. Srivastava, and R. S. Sekhon, 1973: Doppler radar characteristics of precipitation at vertical incidence. *Rev. Geophys. Space Phys.*, **11**, 1-35.

Bolton, D., 1980: The computation of equivalent potential temperature. *Mon. Wea. Rev.*, **108**, 1046-1053.

Cheng, L., and M. English, 1983: A relationship between hailstone concentration and size. *J. Atmos. Sci.*, **40**, 204-213.

———, ———, and R. Wong, 1985: Hailstone size distributions and their relationship to storm thermodynamics. *J. Climate Appl. Meteor.*, **24**, 1059-1067.

Das, P., and M. C. Subba Rao, 1972: The unsaturated downdraught. *Indian J. Meteor. Geophys.*, **23**, 135-144.

Davies-Jones, R. P., 1982: A new look at the vorticity equation with application to tornadogenesis. *Proc. 12th Conf. Severe Local Storms*, San Antonio, TX, Amer. Meteor. Soc., 249-252.

———, 2000: Can the hook echo instigate tornadogenesis barotropically? *Proc. 20th Conf. Severe Local Storms*, Orlando, FL, Amer. Meteor. Soc., 269-272.

———, and H. Brooks, 1993: Mesocyclogenesis from a theoretical perspective. *The Tornado: Its Structure, Dynamics, Prediction, and Hazards, Geophys. Monogr.*, No. 79, Amer. Geophys. Union, 105-114.

———, R. J. Trapp, and H. B. Bluestein, 2001: Tornadoes and tornadic storms. *Severe Convective Storms, Meteor. Monogr.*, No. 50, Amer. Meteor. Soc., 167-221.

Emanuel, K. A., 1994: *Atmospheric Convection*. Oxford University Press, 580 pp.

Houze, R. A., Jr., 1993: *Cloud Dynamics*. International Geophysical Series, Vol. 53, Academic Press, 573 pp.

Kamburova, P. L., and F. H. Ludlam, 1966: Rainfall evaporation in thunderstorm downdraughts. *Quart. J. Roy. Meteor. Soc.*, **92**, 510-518.

Knupp, K. R., and W. R. Cotton, 1985: Convective cloud downdraft structure: An interpretive study. *Rev. Geophys.*, **23**, 183-215.

Lemon, L. R., and C. A. Doswell III, 1979: Severe thunderstorm evolution and mesocyclone structure as related to tornadogenesis. *Mon. Wea. Rev.*, **107**, 1184-1197.

Markowski, P. M., 2002: Hook echoes and rear-flank downdrafts: A review. *Mon. Wea. Rev.*, **130**, 852-876.

———, J. M. Straka, and E. N. Rasmussen, 2002: Direct surface thermodynamic observations within the rear-flank downdrafts of nontornadic and tornadic supercells. *Mon. Wea. Rev.*, **130**, 1692-1721.

———, C. Hannon, J. Frame, E. Lancaster, A. Pietrycha, R. Edwards, and R. L. Thompson, 2003: Characteristics of vertical wind profiles near supercells obtained from the Rapid Update Cycle. *Wea. Forecasting*, **18**, 1262-1272.

Moller, A. R., C. A. Doswell III, M. P. Foster, and G. R. Woodall, 1994: The operational recognition of supercell thunderstorm environments and storm structures. *Wea. Forecasting*, **9**, 327-347.

Ogura, Y., and T. Takahashi, 1971: Numerical simulation of the life cycle of a thunderstorm cell. *Mon. Wea. Rev.*, **99**, 895-911.

———, and ———, 1973: The development of warm rain in a cumulus model. *J. Atmos. Sci.*, **30**, 262-277.

Rasmussen, E. N., 2003: Refined supercell and tornado forecast parameters. *Wea Forecasting*, **18**, 530-535.

———, and D. O. Blanchard, 1998: A baseline climatology of sounding-derived supercell and tornado forecast parameters. *Wea. Forecasting*, **13**, 1148-1164.

Rasmussen, R. M., and A. J. Heymsfield, 1987: Melting and shedding of graupel and hail. Part I: Model physics. *J. Atmos. Sci.*, **44**, 2754-2763.

———, V. Levizzani, and H. R. Pruppacher, 1984: A wind tunnel and theoretical study on the melting behavior of atmospheric ice particles. III: Experiment and theory for spherical ice particles of radius > 500 μm. *J. Atmos. Sci.*, **41**, 381-388.

Richner, H., and P. Viatte, 1995: The hydrostatic equation in the evaluation algorithm for radiosonde data. *J. Atmos. Oceanic Technol.*, **12**, 649-656.

Rogers, R. R., and M. K. Yau, 1989: *A Short Course in Cloud Physics*. International Series in Natural Philosophy, Vol. 113, Pergamon Press, 293 pp.

Rotunno, R., and J. B. Klemp, 1985: On the rotation and propagation of simulated supercell thunderstorms. *J. Atmos. Sci.*, **42**, 271-292.

Soong, S.-T., and Y. Ogura, 1973: A comparison between axisymmetric and slab-symmetric cumulus cloud models. *J. Atmos. Sci.*, **30**, 879-893.

Srivastava, R. C., 1985: A simple model of evaporatively driven downdraft: Application to microburst downdraft. *J. Atmos. Sci.*, **42**, 1004-1023.

———, 1987: A model of intense downdrafts driven by the melting and evaporation of precipitation. *J. Atmos. Sci.*, **44**, 1752-1773.

Thompson, R. L., R. Edwards, J. A. Hart, K. L. Elmore, and P. Markowski, 2003: Close proximity soundings within supercell environments obtained from the Rapid Update Cycle. *Wea. Forecasting*, **18**, 1243-1261.

Walko, R. L., 1993: Tornado spin-up beneath a convective cell: Required basic structure of the near-field boundary layer winds. *The Tornado: Its Structure, Dynamics, Prediction, and Hazards, Geophys. Monogr.*, No. 79, Amer. Geophys. Union, 89-95.